

Multiple-wavelength double random phase encoding with CCD-plane sparse-phase multiplexing for optical information verification

Wen Chen^{1,2,*}

¹*Department of Electronic and Information Engineering,
The Hong Kong Polytechnic University, Hong Kong, China*

²*Department of Electrical and Computer Engineering,
National University of Singapore, Singapore 117583, Singapore*

*Corresponding author: owen.chen@polyu.edu.hk

Received Month X, XXXX; revised Month X, XXXX; accepted Month X, XXXX; posted Month X, XXXX (Doc. ID XXXXXX); published Month X, XXXX

A novel method is proposed by using multiple-wavelength double random phase encoding (MW-DRPE) with CCD-plane sparse-phase multiplexing for optical information verification. Two different strategies are applied to conduct sparse-phase multiplexing in the CCD plane. The results demonstrate that large capacity can be achieved for optical multiple-image verification. The proposed optical verification strategy is implemented based on optical encoding, and the keys generated by optical encryption can further guarantee the safety of the designed optical multiple-image verification system. The proposed method provides a novel alternative for DRPE-based optical information verification. © 2015 Optical Society of America
OCIS codes: (200.4560) Optical data processing; (100.4998) Pattern recognition, optical security and encryption.

1. Introduction

With a rapid development of modern technologies, information security has been considered as one of the most important topics. Since double random phase encoding (DRPE) was proposed [1], optical encoding has attracted more and more attention. In DRPE system, the input image can be converted into stationary white noise [1] by using two statistically-independent phase-only masks placed in the input image plane and Fourier domain, respectively. Its marked advantages [2–4], such as parallel processing and multiple dimensions, have been successfully illustrated. Various algorithms and infrastructures [2–7], such as fully-phase [5] and Fresnel transform [6], have also been developed.

It has been found that under some assumptions, it may be possible for the attackers [8–10] to extract the approximated principal keys, i.e., phase-only masks. Although additional keys are integrated into DRPE system [11,12], its linear characteristic has not been effectively changed. It is desirable that nonlinear strategies can be applied in DRPE system, and a higher security can be achieved without highly increasing system complexity. Photon-counting DRPE [13–16] has been applied as an alternative, however a simple implementation method has not been studied for optical multiple-image verification. Other approaches [17–24] have also been applied to design asymmetric structures and optical multiple-image encoding (or authentication)

systems, however simple strategy using DRPE structure has not been effectively developed and the multiplexing in the CCD plane has not been explored for DRPE-based optical multiple-image verification.

In this paper, a novel and simple method is proposed by using multiple-wavelength double random phase encoding (MW-DRPE) with CCD-plane sparse-phase multiplexing for optical information verification. Two different strategies are developed and applied to conduct sparse-phase multiplexing in the CCD plane. It is found that large capacity can be achieved for optical multiple-image verification, and high security is also guaranteed for the designed optical verification system because of the encoding keys and invisibility of decoded images.

2. Theoretical analysis

Figure 1 shows a schematic setup for the proposed optical system. The DRPE system is applied, and random phase-only masks M1 and M2 are placed at the input image plane and spatial frequency domain, respectively. Let $\exp[j\alpha(x,y)]$ and $\exp[j\beta(\mu,\nu)]$ denote phase-only masks M1 and M2, where $j=\sqrt{-1}$, and $\alpha(x,y)$ and $\beta(\mu,\nu)$ denote 2D maps randomly distributed in the range of $[0, 2\pi]$. Here, free-space wave propagation [6] is applied, however it is straightforward to apply other transform domains, such as fractional Fourier transform [7]. A series

of different input images are encoded based on DRPE system, and different wavelengths are applied for each image encoding. Here, multiple wavelengths are applied as a typical example for illustrating the proposed method, and it can be straightforward to use variable distances. The complex-valued wavefront $O(\xi, \eta)$ obtained in the CCD plane can be described by

$$O_n(\xi, \eta) = \text{FrT}_{\lambda_n, d_2} \left\{ \left(\text{FrT}_{\lambda_n, d_1} \left\{ I_n(x, y) \exp[j\alpha(x, y)] \right\} \right) \times \exp[j\beta(\mu, \nu)] \right\}, \quad (1)$$

where $I_n(x, y)$ denotes input images ($n=1, \dots, N$), FrT denotes free-space wave propagation [6, 25], d_1 and d_2 denote axial distances, and λ_n denotes light wavelength. In practice, complex-valued wavefronts $O_n(\xi, \eta)$ can be obtained by using various optical methods, such as holography [2]. In this study, only phase component is reserved in the CCD plane and used for the decoding, and phase component can be extracted as follows:

$$P_n(\xi, \eta) = PR[O_n(\xi, \eta)] \\ = O_n(\xi, \eta) / |O_n(\xi, \eta)|, \quad (2)$$

where PR denotes phase reservation operation, $||$ denotes modulus operation, and $P_n(\xi, \eta)$ denotes the phase component extracted in the CCD plane. It is worth noting that amplitude part of $O_n(\xi, \eta)$ is not reserved, and is not used for the decoding.

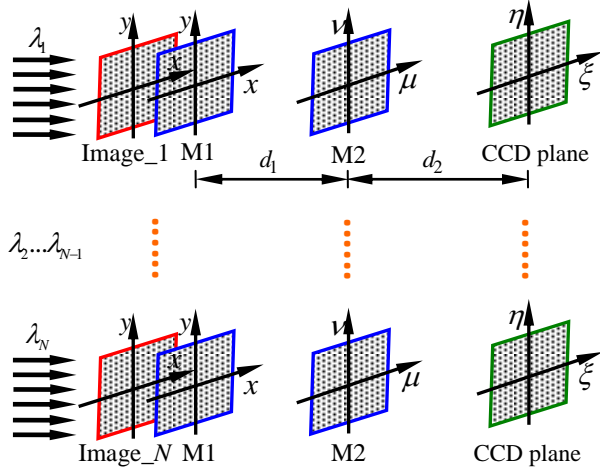


Fig. 1. (Color online) A schematic setup for optical encoding: CCD, charge-coupled device; M1 and M2, random phase-only masks. Symbols $\lambda_1 - \lambda_N$ denote light wavelengths, and d_1 and d_2 denote axial distances. Symbol N denotes the maximum number of the input image. Phase-only mask M1 is placed just behind the input image, and M1 and M2 can be adjusted as the same for encoding different input images.

Since multiple input images are encoded based on DRPE system, a series of phase maps, i.e., $P_n(\xi, \eta)$, are correspondingly obtained in the CCD plane. Subsequently, two different strategies are applied to conduct sparse-phase multiplexing in the CCD plane.

Method 1:

$$PS(\xi, \eta) = \sum_{n=1}^N P_n(\xi, \eta) S_n(\xi, \eta), \quad (3)$$

$$PSA(\xi, \eta) = \begin{cases} PS(\xi, \eta) / |PS(\xi, \eta)| & \text{if } PS(\xi, \eta) \neq 0 \\ 0 & \text{if } PS(\xi, \eta) = 0 \end{cases}, \quad (4)$$

where $PSA(\xi, \eta)$ denotes the synthesized phase map obtained by method 1, and $S_n(\xi, \eta)$ denotes the sparsity map (512×512 pixels) for an extracted phase map. For instance, in one typical sparsity map, only few pixels (such as 40.0%) are useful, and values of these useful pixels are set as one (others are zero). Several sparsity maps are applied, which are mutually independent and not related. Although the total number of useful pixels can be the same, positions of selected and useful pixels are random, i.e., due to $S_n(\xi, \eta)$.

Method 2:

$$\hat{P}(\xi, \eta) = \prod_{n=1}^N P_n(\xi, \eta), \quad (5)$$

$$PSM(\xi, \eta) = S(\xi, \eta) \hat{P}(\xi, \eta), \quad (6)$$

where $PSM(\xi, \eta)$ denotes the synthesized phase map obtained by method 2, and $S(\xi, \eta)$ denotes a sparsity map. Since multiplication operation is involved in method 2, a phase key in the CCD plane should be individually generated for the decoding of each input image. The series of phase keys are generated as follows:

$$K_i(\xi, \eta) = \text{conj} \left[\prod_{n=1, n \neq i}^N P_n(\xi, \eta) \right], \quad (7)$$

where integer $i=1, 2, \dots, N$, and conj denotes complex conjugate.

During optical recovery, the collimated plane wave is generated for the illumination, and the synthesized phase-only map is considered as the ciphertext. Figure 2 shows a schematic setup for the decoding. Since two different sparse-phase multiplexing methods are employed and respectively described by

$$\hat{I}_n(x, y) = \left| \text{FrT}_{\lambda_n, -d_1} \left(\left(\text{FrT}_{\lambda_n, -d_2} [PSA(\xi, \eta)] \right) \times \left\{ \exp[j\beta(\mu, \nu)] \right\}^* \right) \right|, \quad (8)$$

$$\hat{I}_n(x, y) = \left| \text{FrT}_{\lambda_n, -d_1} \left(\left(\text{FrT}_{\lambda_n, -d_2} \left[\text{PSM}(\xi, \eta) K_i(\xi, \eta) \right] \right) \times \left\{ \exp \left[j \beta(\mu, \nu) \right] \right\}^* \right) \right| \quad (i = n), \quad (9)$$

where $\hat{I}_n(x, y)$ denotes the decoded images, asterisk denotes complex conjugate, and $\text{FrT}_{\lambda_n, -d_1}$ and $\text{FrT}_{\lambda_n, -d_2}$ denote free-space wave back-propagation [6,25]. Since only sparse phase map in the CCD plane is reserved for optical decoding, recovered images will not visually render any useful information. Here, nonlinear correlation algorithm [13,17,26,27] is further applied to verify the decoded images, however it could be straightforward to apply other correlation algorithms [28,29]. Nonlinear correlation outputs are generated by [13,17,26,27]

$$C_n(x, y) = \left| \text{IFT} \left(\left| \left\{ \text{FT} [I_n(x, y)] \right\} \left\{ \text{FT} [\hat{I}_n(x, y)] \right\}^* \right|^{w-1} \times \left\{ \text{FT} [I_n(x, y)] \right\} \left\{ \text{FT} [\hat{I}_n(x, y)] \right\}^* \right) \right|^2, \quad (10)$$

where w denotes strength of applied nonlinearity [13,17,26,27], and FT and IFT respectively denote Fourier transform and inverse Fourier transform. To illustrate the proposed method, a flow chart is further shown in Fig. 3.

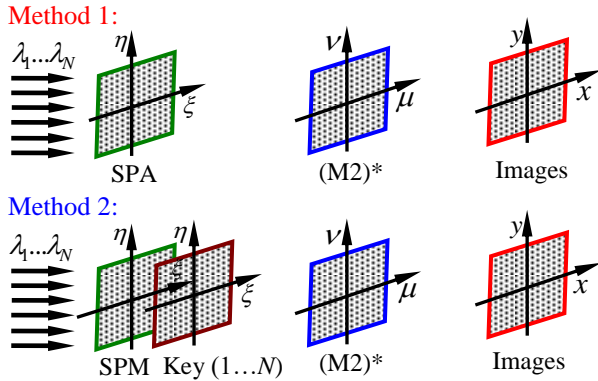


Fig. 2. (Color online) A schematic decoding setup for illustrating method 1 and method 2: asterisk, complex conjugate; SPA, synthesized phase map by method 1; SPM, synthesized phase map by method 2. In method 2, one specific phase key, i.e., $K_i(\xi, \eta)$, should be available for each image recovery, which is placed just behind the synthesized phase map (SPM).

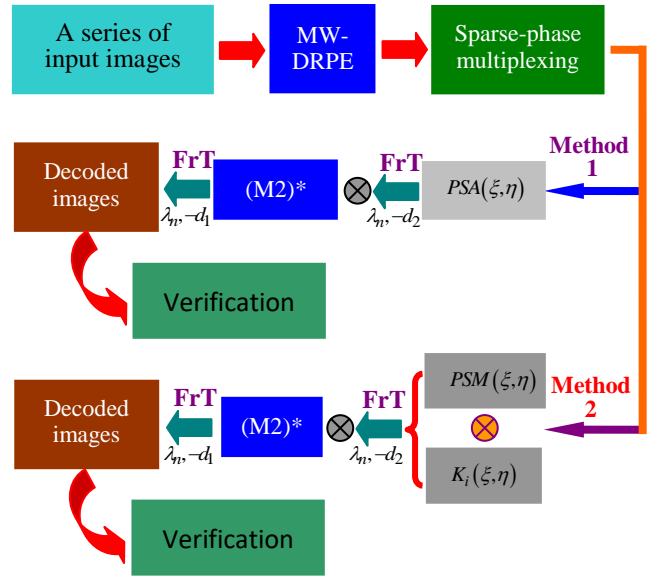


Fig. 3. (Color online) Flow chart for the proposed optical encoding and verification system: Symbol “ \otimes ” denotes a multiplication operation, and asterisk denotes complex conjugate.

3. Results and discussion

The setups shown in Figs. 1 and 2 are conducted to illustrate validity of the proposed optical system. A collimated plane wave is generated for the illumination during optical encoding and decoding, and the series of light wavelengths is $[630 - 20 \times (n-1), n=1, 2, \dots, N]$ nm. Phase-only masks M1 and M2 are randomly distributed in the range of $[0, 2\pi]$, and axial distances d_1 and d_2 are 60.0 mm and 90.0 mm, respectively. Unlike conventional DRPE [1], only phase distributions are extracted and maintained in the CCD plane, and either a digital or optical approach could be used during the decoding. Pixel size of $4.65 \mu\text{m}$ and pixel number of 512×512 are employed during the recordings. In practical applications, the synthesized phase maps, i.e., $\text{PSA}(\xi, \eta)$ or $\text{PSM}(\xi, \eta)$, can be embedded into spatial light modulator controlled by the computer, and multiple images can be sequentially recovered by using different wavelengths. Due to laboratory resource limits, numerical work is conducted to illustrate feasibility and effectiveness of the proposed methods. In practical experiments, influence from setup noise and cross-talk of spatial light modulators can be further analyzed.

Three gray-scale input images (8 bits and 512×512 pixels), i.e., Goodhill, Barbaba and Baboon (selected from USC-SIPI image database <http://sipi.usc.edu/database/database.php?volume=misc>), are encoded by the proposed method. With the two sparse-phase multiplexing methods, synthesized phase maps $\text{PSA}(\xi, \eta)$ and $\text{PSM}(\xi, \eta)$ are obtained and respectively

shown in Figs. 4(a) and 4(b). It can be seen in Figs. 4(a) and 4(b) that only one phase distribution is required and used as ciphertext. In method 1, only 40.0% pixels in each sparsity map $S_n(\xi, \eta)$ have the value of one, and the synthesized phase map $PSA(\xi, \eta)$ can be directly applied without other keys in the CCD plane. In method 2, only 15.0% pixels in the sparsity map $S(\xi, \eta)$ have the value of one, and a specific phase key [see Eq. (7)] is also generated for each image decoding.

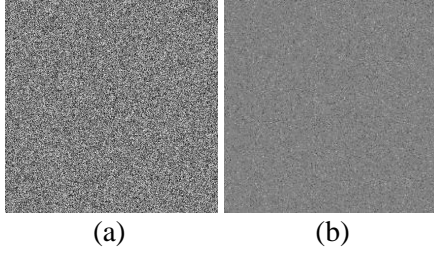


Fig. 4. Synthesized phase maps (a) $PSA(\xi, \eta)$ and (b) $PSM(\xi, \eta)$.

Figures 5(a)–5(c) show the recovered images (corresponding to the three different input images), when the synthesized phase map $PSA(\xi, \eta)$ is applied and the first strategy (method 1) is considered. In this case, setup parameters, such as wavelengths and distances, are correctly applied for each image decoding. In practice, different evaluation parameters [30–45] can be calculated to evaluate quality of decoded images. In this study, mean squared error (MSE) [41] is calculated and applied to evaluate quality of recovered images, and the MSEs for Figs. 5(a)–5(c) are 1.48×10^4 , 1.47×10^4 and 1.83×10^4 , respectively. It can be seen in Figs. 5(a)–5(c) that no information about input images can be visually observed. Figures 5(d)–5(f) show the generated nonlinear correlation maps corresponding to Figs. 5(a)–5(c), respectively. It can be seen in Figs. 5(d)–5(f) that since the decoded images still contain some invisible but useful information, one remarkable peak can be observed in each correlation distribution. When the keys, such as phase-only mask M2, wavelength and distances, are incorrectly used during the decoding, only noisy background can be obtained in the generated nonlinear correlation maps. Figures 5(g)–5(i) show the generated nonlinear correlation maps, when phase-only mask M2 is incorrectly applied for respectively recovering the three different input images. It can be seen in Figs. 5(g)–5(i) that when key is wrong, no remarkable peaks can be observed in the generated nonlinear correlation distributions. It is illustrated that the optical verification system can be established based on optical encryption, and the keys generated during the encoding can also be used for guaranteeing optical verification system. For the sake of brevity, performance of other keys is not presented here.

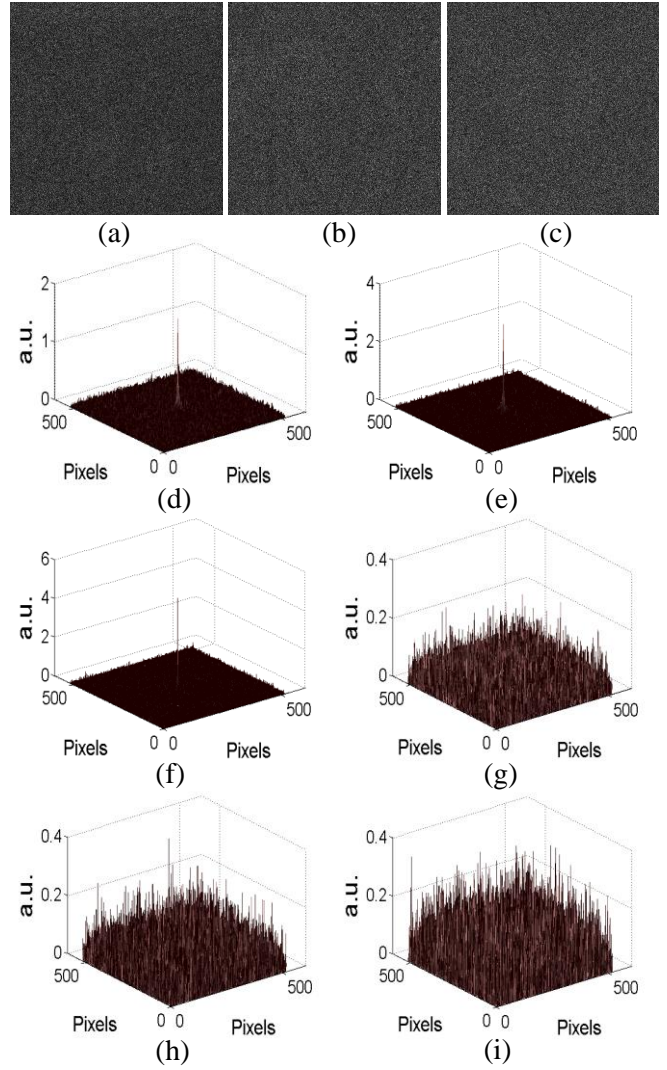


Fig. 5. (Color online) (a)–(c) The recovered images obtained when the synthesized phase map $PSA(\xi, \eta)$ is applied and the first strategy (method 1) is considered, (d)–(f) the generated nonlinear correlation maps respectively corresponding to (a)–(c). (g)–(i) The generated nonlinear correlation maps, when phase-only mask M2 is incorrectly applied for recovering the three different input images.

Figures 6(a)–6(c) show the recovered images (corresponding to the three different input images), when the synthesized phase map $PSM(\xi, \eta)$ is applied and the second strategy (method 2) is considered. In this case, setup parameters and phase key $K_i(\xi, \eta)$ are correctly applied for each image recovery. The MSEs for Figs. 6(a)–6(c) are 1.49×10^4 , 1.48×10^4 and 1.84×10^4 , respectively. It can be seen in Figs. 6(a)–6(c) that the decoded images do not directly render any information about the input images. Figures 6(d)–6(f) show the generated nonlinear correlation maps corresponding to Figs. 6(a)–6(c),

respectively. Since a phase key $K_i(\xi, \eta)$ is also applied, the correctly sparse phase map without cross-talk term is generated in the CCD plane for each recovery. Hence, the higher sparsity levels, such as 15.0%, can be used compared with that in method 1. The phase key should be generated for each image decoding, which also enhances system security. However, in method 1, only one ciphertext (i.e., synthesized phase map) is required, and the implementation may be more straightforward without phase keys in the CCD plane. The performance of keys is also analyzed. Figures 6(g)–6(i) show the generated nonlinear correlation maps, when phase-only mask M2 is incorrectly applied for respectively recovering the three different input images. It is illustrated that in method 2, the keys should be correctly applied to conduct the correct verification. For brevity, performance of other parameters, such as wavelength and axial distances, is not presented here.

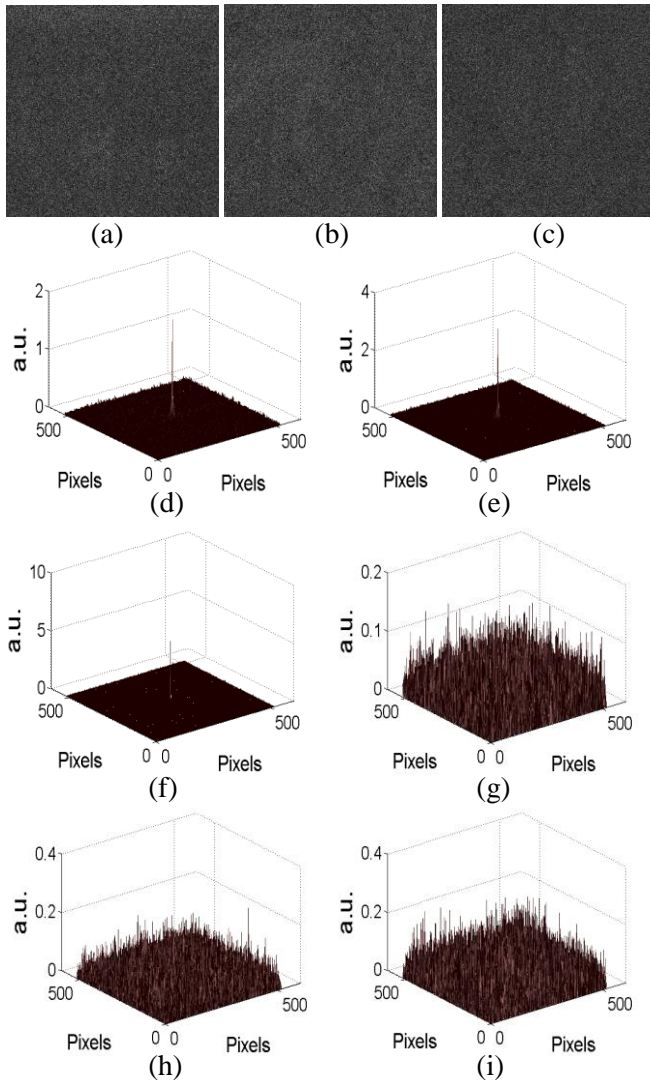


Fig. 6. (Color online) (a)–(c) The recovered images obtained when the synthesized phase map $PSM(\xi, \eta)$ is applied and the second strategy (method 2) is considered,

(d)–(f) the generated nonlinear correlation maps respectively corresponding to (a)–(c). (g)–(i) The generated nonlinear correlation maps, when phase-only mask M2 is incorrectly applied for recovering the three different input images.

Capacity of the proposed method is further analyzed by encoding a larger number of input images into only one synthesized phase map. Figure 7(a) shows one typical correlation (i.e., verification) distribution, when 6 different grayscale input images (each image with 8 bits) are encoded and method 1 is considered. In this case, each sparsity map $[S_n(\xi, \eta) \ n=1,2...6]$ randomly contains 70.0% of 512×512 pixels. Figure 7(b) shows one typical authentication distribution, when 6 different grayscale input images (8 bits) are encoded and method 2 is considered. In this case, the sparsity map $S(\xi, \eta)$ still contains only 15.0% of 512×512 pixels. It can be seen in Figs. 7(a) and 7(b) that the proposed method possesses high capacity, and method 2 can achieve the larger capacity because of the use of one specific phase key in the CCD plane for each image decoding. To use visible light source, the maximum number of input images is around 16 in the second method, when an interval of 20 nm in the wavelength is applied. In method 1, cross-talk terms will be generated due to direct superposition of sparse-phase information in the CCD plane, and the system capacity is limited. When more input images (such as more than 6) are encoded, each sparsity map should contain more useful pixels (i.e., the pixel value equivalent to one). In practice, different sparsity levels can be arbitrarily adjusted for encoding each input image to ensure that all recovered images can be effectively verified without visual observation of input images. The first method is more suitable when only a few input images, such as less than 7, are simultaneously encoded. In this case, no additional security keys should be generated and transmitted to the receiver. The second method is more suitable when the larger number of input images, such as more than 6, should be simultaneously encoded. However, an additional phase key should be generated for each authorized receiver, which may request more effort.

It is worth noting that different from conventional DRPE [1], the objective of this study is not to extract high-quality input images during the decoding. Instead, the decoded images can be verified without the disclosure of original information, and an additional security layer can be established. Different from conventional optical encoding strategies [1–7], in this study optical multiple-image verification system is established based on optical encoding, and the keys generated by optical encoding (i.e., in method 2) further guarantee the safety of the designed optical verification system.

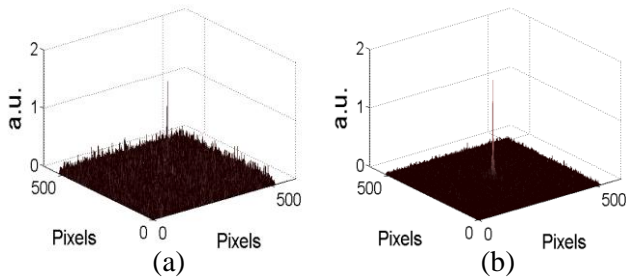


Fig. 7. (Color online) (a) One typical verification distribution obtained when 6 different grayscale input images are encoded and method 1 is considered; and (b) one typical verification distribution obtained when 6 different grayscale input images are encoded and method 2 is considered.

4. Conclusions

A novel method has been proposed by using the MW-DRPE with CCD-plane sparse-phase multiplexing for optical multiple-image verification. Two different strategies are developed and applied to conduct sparse-phase multiplexing in the CCD plane, and main advantages of the proposed optical system have been illustrated. The results demonstrate that large capacity can be achieved for optical multiple-image verification, and high security can be correspondingly guaranteed for the designed optical multiple-image verification system, i.e., encoding keys and without direct observation of input images. The proposed method provides a novel alternative for DRPE-based optical image processing.

This work was supported by the Singapore MINDEF-NUS Joint Applied R&D Cooperation Programme (JPP) Project: MINDEF/NUS/JPP/14/01/02.

References

1. P. Refregier and B. Javidi, "Optical image encryption based on input plane and Fourier plane random encoding," *Opt. Lett.* **20**, 767–769 (1995).
2. O. Matoba, T. Nomura, E. P. Cabré, M. S. Millán, and B. Javidi, "Optical techniques for information security," *Proc. IEEE* **97**, 1128–1148 (2009).
3. B. Javidi and T. Nomura, "Securing information by use of digital holography," *Opt. Lett.* **25**, 28–30 (2000).
4. W. Chen, X. Chen, and Colin J. R. Sheppard, "Optical image encryption based on diffractive imaging," *Opt. Lett.* **35**, 3817–3819 (2010).
5. B. Javidi and A. Sergent, "Fully phase encoded key and biometrics for security verification," *Opt. Eng.* **36**, 935–942 (1997).
6. O. Matoba and B. Javidi, "Encrypted optical memory system using three-dimensional keys in the Fresnel domain," *Opt. Lett.* **24**, 762–764 (1999).

7. G. Unnikrishnan, J. Joseph, and K. Singh, "Optical encryption by double-random phase encoding in the fractional Fourier domain," *Opt. Lett.* **25**, 887–889 (2000).
8. A. Carnicer, M. M. Usategui, S. Arcos, and I. Juvells, "Vulnerability to chosen-cyphertext attacks of optical encryption schemes based on double random phase keys," *Opt. Lett.* **30**, 1644–1646 (2005).
9. W. Stallings, *Cryptography and Network Security: Principles and Practice*, 4th ed. (Prentice Hall, New Jersey, 2006).
10. Y. Frauel, A. Castro, T. J. Naughton, and B. Javidi, "Resistance of the double random phase encryption against various attacks," *Opt. Express* **15**, 10253–10265 (2007).
11. B. Hennelly and J. T. Sheridan, "Optical image encryption by random shifting in fractional Fourier domains," *Opt. Lett.* **28**, 269–271 (2003).
12. P. Kumar, A. Kumar, J. Joseph, and K. Singh, "Impulse attack free double-random-phase encryption scheme with randomized lens-phase functions," *Opt. Lett.* **34**, 331–333 (2009).
13. E. Pérez-Cabré, M. Cho, and B. Javidi, "Information authentication using photon-counting double-random-phase encrypted images," *Opt. Lett.* **36**, 22–24 (2011).
14. M. Cho and B. Javidi, "Three-dimensional photon counting double-random-phase encryption," *Opt. Lett.* **38**, 3198–3201 (2013).
15. A. Markman and B. Javidi, "Full-phase photon-counting double-random-phase encryption," *J. Opt. Soc. Am. A* **31**, 394–403 (2014).
16. S. K. Rajput, D. Kumar, and N. K. Nishchal, "Photon counting imaging and phase mask multiplexing for multiple images authentication and digital hologram security," *Appl. Opt.* **54**, 1657–1666 (2015).
17. W. Chen and X. Chen, "Optical multiple-image authentication based on modified Gerchberg-Saxton algorithm with random sampling," *Opt. Commun.* **318**, 128–132 (2014).
18. D. Fan, X. F. Meng, Y. Wang, X. Yang, X. Pan, X. Peng, W. He, G. Dong, and H. Chen, "Multiple-image authentication with a cascaded multilevel architecture based on amplitude field random sampling and phase information multiplexing," *Appl. Opt.* **54**, 3204–3215 (2015).
19. X. Y. Liang, X. Su, S. Li, X. Liu, and S. Zeng, "Key rotation multiplexing for multiple-image optical encryption in the Fresnel domain," *Opt. Laser Technol.* **43**, 889–894 (2011).
20. X. Peng, H. Wei, and P. Zhang, "Asymmetric cryptography based on wavefront sensing," *Opt. Lett.* **31**, 3579–3581 (2006).
21. H. T. Chang, H. E. Hwang, C. L. Lee, and M. T. Lee, "Wavelength multiplexing multiple-image encryption using cascaded phase-only masks in the Fresnel transform domain," *Appl. Opt.* **50**, 710–716 (2011).
22. H. T. Chang, H. E. Hwang, and C. L. Lee, "Position multiplexing multiple-image encryption using cascaded phase-only masks in Fresnel transform domain," *Opt. Commun.* **284**, 4146–4151 (2011).
23. H. E. Hwang, H. T. Chang, and W. N. Lie, "Multiple-image encryption and multiplexing using a modified Gerchberg-Saxton algorithm and phase modulation in Fresnel-transform domain," *Opt. Lett.* **34**, 3917–3919 (2009).
24. X. Pan, X. Meng, Y. Wang, X. Yang, X. Peng, W. He, G. Dong, and H. Chen, "A kind of multilevel authentication system for multiple-image by modulated real part synthesis and iterative phase multiplexing," *J. Modern Opt.* DOI: 10.1080/09500340.2015.1088585, 2015.
25. J. W. Goodman, *Introduction to Fourier Optics*, 2nd ed. (McGraw-Hill, New York, 1996).
26. B. Javidi, "Nonlinear joint power spectrum based optical correlation," *Appl. Opt.* **28**, 2358–2367 (1989).

27. W. Chen and X. Chen, "Ghost imaging for three-dimensional optical security," *Appl. Phys. Lett.* **103**, 221106 (2013).
28. M. S. Millán, E. Pérez-Cabré, and B. Javidi, "Multifactor authentication reinforces optical security," *Opt. Lett.* **31**, 721–723 (2006).
29. F. Sadjadi and B. Javidi, *Physics of Automatic Target Recognition* (Springer, New York, 2007).
30. Y. Shi, T. Li, Y. Wang, Q. Gao, S. Zhang, and H. Li, "Optical image encryption via ptychography," *Opt. Lett.* **38**, 1425–1427 (2013).
31. Y. Zhang and B. Wang, "Optical image encryption based on interference," *Opt. Lett.* **33**, 2443–2445 (2008).
32. W. Qin and X. Peng, "Asymmetric cryptosystem based on phase-truncated Fourier transforms," *Opt. Lett.* **35**, 118–120 (2010).
33. X. Wang and D. Zhao, "Multiple-image encryption based on nonlinear amplitude-truncation and phase-truncation in Fourier domain," *Opt. Commun.* **284**, 148–152 (2011).
34. G. Situ and J. Zhang, "Position multiplexing for multiple-image encryption," *J. Opt. A: Pure Appl. Opt.* **8**, 391–397 (2006).
35. J. Liu, X. Xu, Q. Wu, J. T. Sheridan, and G. Situ, "Information encryption in phase space," *Opt. Lett.* **40**, 859–862 (2015).
36. Y. Qin, Q. Gong, and Z. Wang, "Simplified optical image encryption approach using single diffraction pattern in diffractive-imaging-based scheme," *Opt. Express* **22**, 21790–21799 (2014).
37. X. F. Meng, L. Z. Cai, X. F. Xu, X. L. Yang, X. X. Shen, G. Y. Dong, and Y. R. Wang, "Two-step phase-shifting interferometry and its application in image encryption," *Opt. Lett.* **31**, 1414–1416 (2006).
38. G. Situ and J. Zhang, "Multiple-image encryption by wavelength multiplexing," *Opt. Lett.* **30**, 1306–1308 (2005).
39. W. Chen and X. Chen, "Double random phase encoding using phase reservation and compression," *J. Opt.* **16**, 025402 (2014).
40. W. Chen, B. Javidi, and X. Chen, "Advances in optical security systems," *Adv. Opt. Photon.* **6**, 120–155 (2014).
41. W. Chen, X. Chen, A. Anand, and B. Javidi, "Optical encryption using multiple intensity samplings in the axial domain," *J. Opt. Soc. Am. A* **30**, 806–812 (2013).
42. W. Chen, G. Situ, and X. Chen, "High-flexibility optical encryption via aperture movement," *Opt. Express* **21**, 24680–24691 (2013).
43. W. Chen, X. Chen, A. Stern, and B. Javidi, "Phase-modulated optical system with sparse representation for information encoding and authentication," *IEEE Photon. J.* **5**, 6900113 (2013).
44. W. Chen and X. Chen, "Marked ghost imaging," *Appl. Phys. Lett.* **104**, 251109 (2014).
45. W. Chen and X. Chen, "Grayscale object authentication based on ghost imaging using binary signals," *EPL* **110**, 44002 (2015).